Nanomechanical and nanotribological characterization of microelectromechanical system

M. PUSTAN[a,c*], R. MULLER[b], J.C. GOLINVAL[a]
[a]*Department of Aerospace and Mechanical Engineering, University of Liege, Chemin des Chevreuils 1, B-4000 Liege, Belgium*
[b]*National Institute for Research and Development in Microtechnologies IMT- Bucharest, Erou Iancu Nicolae Str. 126A Ilfov - Voluntari, Ro-077190, Romania*
[c]*Department of Machine Elements and Tribology, Technical University of Cluj-Napoca, Muncii Str. 101-103, Ro-400641 Cluj-Napoca, Romania*

Investigations of the mechanical and tribological properties of microelectromechanical system (MEMS) components on nanoscale can provide insights into failure mechanism of material. The main goal of this paper is focused on the mechanical and tribological characterizations of MEMS mechanical components in order to improve their reliability design. The mechanical properties of interests are stiffness, modulus of elasticity, stress, strain. Dynamical investigations are performed to analyze the resonant frequency response, velocity and amplitude of oscillations of electrostatically actuated microcomponents and to estimate the quality factor. Finite element analysis is used to validate the experimental results of mechanical properties and to simulate the dynamical behaviour of investigated microcomponents. Tribological investigations are developed to estimate the stiction and friction. Testing and the individual characterization of MEMS materials and structures, performed using advanced equipments such as atomic force microscope and optical vibrometer analyzer are presented.

(Received September 8, 2011; accepted April 11, 2012)

Keywords: Flexible microcomponents, Stiffness, Frequency response, Quality factor, Friction and Stiction

1. Introduction

Microelectromechanical Systems (MEMS) combine integrated mechanical structure and low-power electronic components. The MEMS specific technologies, already partly standardized and available for industrial mass production, are developed based on microelectronics technology, supplemented with special micromachining techniques.

MEMS devices can be classified based on their applications in:

- Microsensors used to detect physical or environmental changes as pressure sensor, gyroscope, inertial sensor, chemical sensor, gas sensor, accelerometer, motion sensor, thermal sensor and optical sensor.
- Microactuators used to activate the other MEMS components as electrostatic actuators, thermal stimulus actuators.
- Radio frequency MEMS (RF-MEMS) used to switch, transmit, filter and manipulate radio frequency signals as metal-to-metal or ohmic RF switches, tunable capacitor, tunable filter, micro-resonators.
- Optical MEMS designed to reflect, filter, or amplify light as optical reflectors, micromirrors, optical switches, optical attenuators.
- Microfluidic MEMS designed to interact with fluid-based system as micropumps, microvalves.
- Bio MEMS designed to interact with biological samples (proteins, biological cells, medical reagents) as microfluidic chips, intra-vascular devices, and DNA chip.

The widespread growth and acceptance of the MEMS technology in diverse applications from customer electronics to space and military hinges on products, achieving a suitable balance of quality and cost. Quality essentially implies that a product performs as specified in the datasheet, which means, it performs reliably. The reliability and the lifetime are crucial parameters in different MEMS applications and these are strongly dependent on the material properties [1 -6]. More, MEMS devices need to be designed to perform their expected functions with short duration, typically in milliseconds to picoseconds timescale. This accuracy in response of MEMS is influenced by the material properties.

To improve the stability and reliability of the MEMS devices, numerous new characterization and testing methods have been developed, but still many more are required for better fundamental understanding of the failure mechanisms.

The research in the MEMS materials characterization is carried out worldwide and an e-database has been set up at the MEMS Clearinghouse web site (http://www.memsnet.org/material). The correct material selection criteria are essential when designing MEMS structures. Many MEMS designers still do not take into account the implications that the scale difference and inaccurate material properties have on reliability when designing new devices. The material properties and failure

mechanisms can be substantially different from the macro scale to the micro scale. Additionally, the material properties on microcomponents depend on the fabrication conditions. Based on the small size of MEMS components, crack related mechanisms and surface effects are much more significant in these devices. Stiction and friction can build up high local stress field in MEMS devices with movable parts. Therefore, materials and failure mechanisms that are fairly well characterized on the macro scale require future investigations using micromachined test structures.

The mechanical characteristics of microcomponents have an importance influence on reliability and performance of MEMS. The stiffness and modulus of elasticity are needed to predict the deformations in the elastic regime. The stress and strain are necessary to anticipate the acceptable operating limits. The resonant frequency and amplitude of vibrations have a direct influence on oscillating mode of MEMS resonators. Theoretical and experimental analyses have then to be developed to analyze the mechanical behaviour of MEMS components and improve their reliability design.

The most important and unavoidable problems in MEMS are stiction and fatigue [1, 4, 7, 8]. Stiction has a great influence on the performance and reliability of MEMS devices with movable components. Fatigue of vibrating MEMS structures can manifest itself more as the loss in the accuracy of response than the crack propagations.

The atomic force microscope (AFM) can be used satisfactorily to evaluate the mechanical characteristics of MEMS components under static loadings, and for surface and tribological characterizations [2, 5, 9, 10]. The spectroscopy in point of AFM is useful to estimate the stiction and the AFM lateral force mode is used to measure the coefficients of friction. The accurate measurements of the flexible microcomponents deflection versus the applied force, which provide information about the sample stiffness, can easily be performed using AFM. The test structure can be statically deflected by an external mechanical load given by the bending of AFM probe or can vibrate at their resonant frequency under an exciting signal, which describes the dynamic response of components. The dynamic response of MEMS components under a cyclic loading gives information about the damping and quality factor, and provides information useful for fatigue characterization [11, 12].

The long term stability and reliability of MEMS devices can be monitored through the change of mechanical properties. The accelerated testing techniques are used to characterize the fatigue of MEMS components. The fatigue is a result of incremental damage accumulated during the load cycles. Any process resulting in an irreversible repositioning of atoms in the material can contribute to fatigue.

Polysilicon, the most frequency used material in surface micromachined structures, is a brittle material with no dislocations movement of atoms prior to fracture. The fatigue mechanism in polysilicon is based on the fatigue of the native oxide layer. The polysilicon has been introduced as the main component in surface micromachined MEMS by researchers at University of California Berkeley in 1980, and has remained since then the main structural material utilized in surface micromachining. The polysilicon is usually deposited by low-presure chemical vapor deposition from silane, which can be combined with phosphane or diborane in order to yield doped film layers possessing electric conductivity. Compared to single crystal silicon, which is anisotropic, the polysilicon is isomorphic, and therefore is amenable to simpler mechanical design. The polysilicon has a Young's modulus of 160GPa (given in literature) and Poisson's ratio of 0.22. It is a linear brittle material with fracture strength as high as 3 GPa [3].

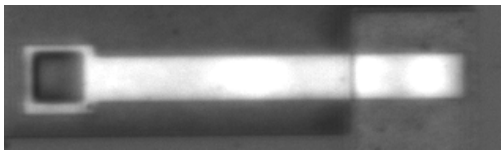

(a)

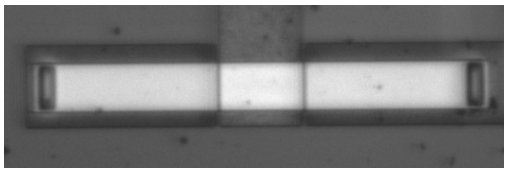

(b)

Fig.1. MEMS mechanical components: (a) Microcantilever, (b) Microbridge.

The mechanical elements composing MEMS resonators are based on microcantilevers and microbridges as presented in Fig.1. Mechanical and tribological investigations of these MEMS mechanical components fabricated from polysilicon are performed using advanced techniques based on optical detection methods and presented in this paper. The article is organized as follow: (*i*) mechanical properties of MEMS structures and materials, determined based on the statically response of beams under mechanical loading are presented in section 2; (*ii*) then, section 3 presents the investigations of the dynamic response of electrostatically actuated MEMS resonator, measurements performed under ambient conditions and in vacuum; (*iii*) in section 4, the tribological investigations of MEMS materials are presented in order to measure the stiction and the coefficient of friction; (*iv*) concluding remarks on the reliability design of MEMS resonators are summarized at the end of paper.

2. Measurement of the mechanical properties of MEMS components

2.1. Bending stiffness

One way to characterize the performance of MEMS flexible components as microbridges and microcantilevers is by defining their relevant stiffness [3, 5, 9, 10, 13].

Stiffness is a fundamental criterion of elastically-deformable mechanical flexible microcomponents. The stiffness of a microcantilever if the force is applied at the beam free-end and of a microbridge if the force is applied at the mid-point can be computed using the following well known relations [3, 9]:

- for a microcantilever

$$k_c = \frac{1}{4}\frac{wt^3}{l^3}E \tag{1}$$

- for a microbridge

$$k_b = 16\frac{wt^3}{l^3}E \tag{2}$$

where w, t and l are the width, thickness and length of samples and E is the Young's modulus of material.

Extraction of the mechanical properties of MEMS materials is possible from dynamic characteristic, such as resonant frequency response of MEMS structures as well as their static response, such as force versus deflection experimental dependence of samples.

In order, to estimate the stiffness of investigated samples, modulus of elasticity, stress and strain an atomic force microscope (AFM) is used. The normal mode of AFM, considering the physical contact between AFM tip and sample, is used to estimate the stiffness based on the next steps:

1) Calibration of the AFM for contact (normal) mode and determination of the real stiffness k_{AFM} of AFM probe using a special etching microspring with know stiffness as presented in Fig.2 [9].

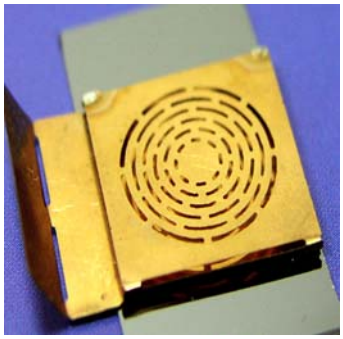

Fig.2. Microspring for AFM probe calibration.

Because the stiffness of AFM probe given by manufacturer has a wide range, the difference between the given value and the real stiffness often exceed 50%. Therefore, for accuracy measurements of the mechanical properties of MEMS components, the real stiffness of AFM probe has to be measured. The AFM probe and the microspring are bending together in the AFM normal mode. The displacement of AFM piezo table is controlled and the bending deflection of AFM probe is optically monitored. The difference between them gives the spring deflection. This deflection of microspring together with its known stiffness gives the force. This force and the bending deflection of AFM probe are used to evaluate the real stiffness of AFM probe.

2) Estimation of the sample stiffness. The succesive positions of the investigated sample and the AFM probe during testing are shown in Fig.3.

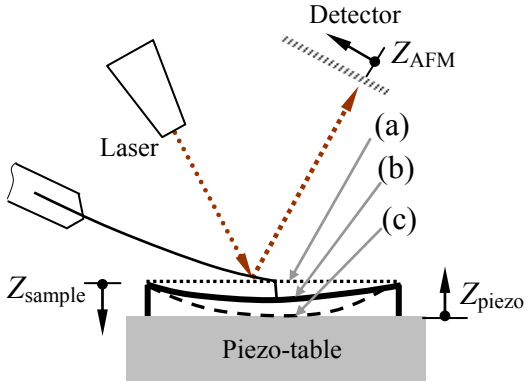

Fig.3. Bending of AFM probe and sample: (a) initial contact between AFM probe and sample; (b) bending of AFM probe and sample; (c) bending only of AFM probe.

The vertical displacement of piezo-table Z_{piezo} is controlled and the deflection of AFM probe Z_{AFM} is optically monitored. Experimental dependences between displacement of piezo-table and deflection of AFM probe as presented in Fig.4 are obtained.

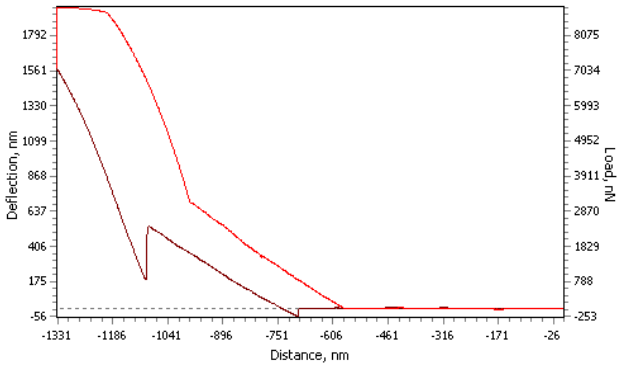

Fig.4. Experimental AFM curve of flexible structures.

An experimental AFM curve has two different slopes as presented in Fig.4. The first part of curve corresponds to the bending of AFM probe and samples (position *b* from Fig.3) and the second part is given by the bending only of AFM probe because the sample sticks to substrate (position *c* from Fig.3).

The real stiffness of AFM probe k_{AFM} is known and using its bending deflection from the second part of curve, the elastic force is computed:

$$F = k_{AFM} \times Z_{AFM} \tag{3}$$

Based on the controlled displacement of AFM piezo-table Z_{piezo} and the monitored deflection of AFM probe Z_{AFM}, the bending deflection of sample is determined:

$$Z_{sample} = Z_{piezo} - Z_{AFM} \tag{4}$$

Considering the equations (3) and (4), the stiffness of investigated microcomponents can be evaluated as:

$$k = \frac{F}{Z_{sample}} \tag{5}$$

The presented method is used to estimate the stiffness of investigated MEMS components presented in Fig.1, fabricated from polysilicon.

The dimensions of samples are the following:

- length $l = 250\mu m$
- width $w = 30\mu m$
- thickness $t = 1.9\mu m$
- the gap between flexible plate and substrate $g_0 = 2\mu m$

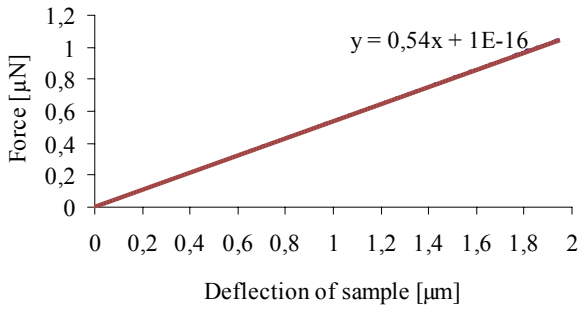

Fig.5. Experimental AFM dependence between deflection of a microcantilever 250×30×1.9µm and force.

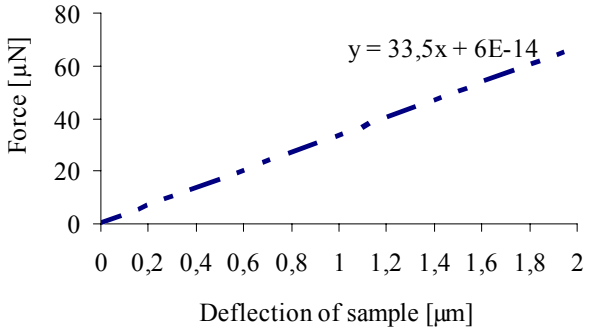

Fig.6. Experimental AFM dependence between deflection of a microbridge 250×30×1.9µm and force.

During experimental tests the AFM tip is positioned at the free-end of microcantilever and at the mid-point of microbridge. The experimental dependence between the bending deflection of microcantilever and the applied force is presented in Fig.5. The tests are performed in cleanroom with 40-45% relative humidity using an NT200 Multifunctional Scanning Probe Microscope and an AFM probe NSC 36/A (www.spmtips.com) with the spring constant given by manufacturer between 0.25 and 2.5 N/m (typical value of 0.95N/m).

The slopes of experimental curves give the sample stiffness. The estimated stiffness is 0.54N/m of the cantilever 250×30×1.9µm close to the theoretical stiffness computed using the relation (1) which is 0.526N/m.

For experimental test of microbridge an AFM probe NSC15/Si3N4 (www.spmtips.com) with the spring constant between 20 and 75N/m (typical value of 40N/m) is used. The force given by the bending deflection of AFM probe and its real stiffness is applied at the mid-point of sample. The experimental dependence between the deflection of microbridge and the force is presented in Fig.6. The experimental stiffness of the investigated microbridge 250×30×1.9µm is 33.5N/m. By using the relation (2) the theoretical stiffness is computed at 33.71N/m for the microbridge, in good agreement with the experimental value.

The differences between the theoretical and experimental results of stiffness of the investigated microcomponents are influenced by the accuracy of the experimental tests, by the differences between the sample dimensions and depend on the material properties. In the theoretical computation, a Young's modulus of polysilicon of 160GPa (taken from literature) is used and it can be different by its real value.

Stiffness of the vibrating MEMS structures can also be determined using the resonant tests, as included in the section 3 of paper. From the resonant frequency response of beam the stiffness can be estimated.

2.2. Modulus of elasticity

The modulus of elasticity can be directly and accurately derived from Hooke's Law. In this paper, a quasi-static method is used to measure the modulus of elasticity of investigated micromechanical flexible structures based on the AFM bending deflection of samples. If the geometrical dimensions are measured and the stiffness of samples is experimental determined the modulus of elasticity of a microcantilever can be experimental-analytical estimated as:

$$E = \frac{4l^3}{wt^3} \cdot \frac{F}{Z_{sample}} \tag{6}$$

For a microbridge, the modulus of elasticity can be determined using the relation:

$$E = \frac{l^3}{16wt^3} \cdot \frac{F}{Z_{sample}} \tag{7}$$

where the applied force F and the resulting deflection of samples are determined using the normal mode of AFM and the methodology described in section 2.1 of paper.

Based on the measured geometrical dimensions of investigated MEMS components and the experimental AFM dates of the applied force and deflections of samples, the modulus of elasticity are determined of 157GPa for the investigated microcantilever and 159GPa of microbridge. In theoretical computation, a value of 160GPa for Young's modulus of polysilicon is considered.

Another quasi-static technique for measuring the Young's modulus is the beam pull-in method. The samples are deflected by an electrostatic force to the pull-in position and the Young's modulus can be extracted from the determined pull-in voltage.

2.3. Stress and strain

The bending of a microcantilever and a microbridge under small deformation produces normal stress. The stress varies linearly over the cross-section going from tension to compression through zero in the neutral axis. The maximum stress values are found on the outer fibers as:

$$\sigma_b = \frac{M_b}{I_y} \cdot \frac{t}{2} \tag{8}$$

where $I_y = w \cdot t^3 / 12$ is the cross – sectional moment of inertia.

Considering the expression of the bending moment given by a force applied at the free-end of microcantilever and at the mid-point of microbridge, based on equation (8) and after performing the necessary calculation, the bending stress of a microcantilever can be computed as:

$$\sigma_b = \frac{6l}{wt^2} F = \frac{3}{2} \frac{tE}{l^2} Z_{sample} \tag{9}$$

and of a microbridge as

$$\sigma_b = \frac{3l}{4wt^2} F = \frac{12tE}{l^2} Z_{sample} \tag{10}$$

Failure in MEMS, as the situation where a microcomponents does no longer perform as expect/design, can occur in the form of yielding for ductile materials where the stresses exceed the yield limit. If the yields stress (σ_y) for a material is known, by using the relation (9) for a microcantilever and (10) for a microbridge, is possible to analyze the following aspects:

a) Verification of the yielding criteria: $\sigma_b \le \sigma_y$

b) Calculation of the minimum thickness of the sample with respect to the yielding criteria:

- for a microcantilever

$$t_{\min} = \left[\frac{6l \cdot F}{w \cdot \sigma_y} \right]^{1/2} \tag{11}$$

- for a microbridge

$$t_{\min} = \left[\frac{3l \cdot F}{4w \cdot \sigma_y} \right]^{1/2} \tag{12}$$

For MEMS designers it is an advantage to have the equations for the calculation of geometrical dimensions of microcomponents considering the yielding criteria.

For elastic materials and small deformations, the stress - strain relationship is linear, and in the case of a microcantilever and a microbridge under bending deformations, the stress and strain are connected by Hooke's Law:

$$\sigma = \varepsilon \cdot E \tag{13}$$

The strain of a microcantilever can be estimated using the relation:

$$\varepsilon = \frac{3t}{2l^2} Z_{sample} \tag{14}$$

and of a microbridge as

$$\varepsilon = \frac{12t}{l^2} Z_{sample} \tag{15}$$

Using the determined experimental value of Young's modulus and the measured geometrical dimensions of investigated samples, the bending stress is experimental-analytical determined based on equation (9) for microcantilever and equation (10) for microbridge, considered the maximum forces which bend the samples to substrate.

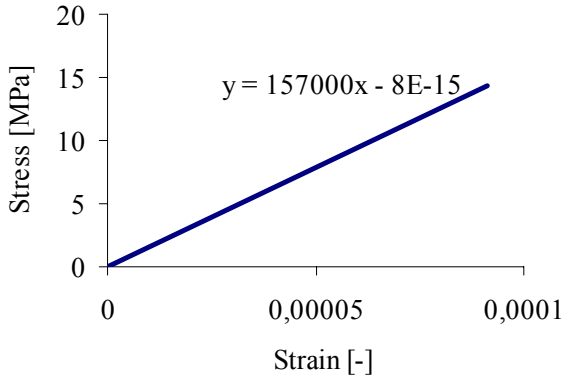

Fig.7. Experimental dependence between stress and strain of a microcantilever 250×30×1.9μm.

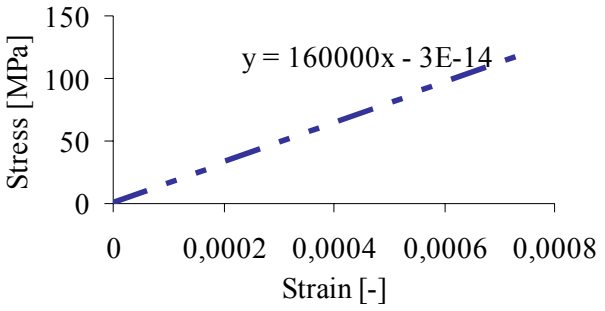

Fig.8. Experimental dependence between stress and strain of a microbridge 250×30×1.9μm.

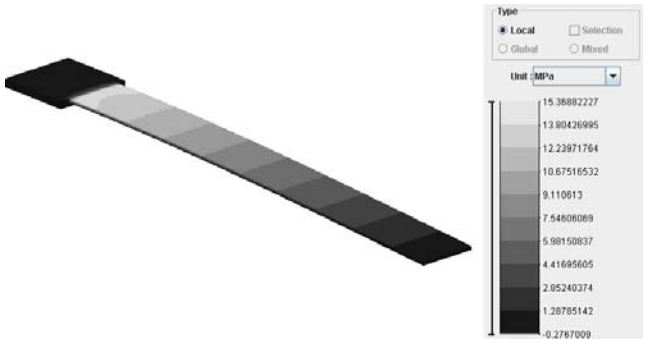

Fig.9. Finite element analysis of the bending stress of a microcantilever 200×30×1.9μm.

Fig.10. Finite element analysis of the bending stress of a microbridge 200×30×1.9μm.

Using the relations (14) and (15), the strains of the investigated beams are experimental- analytical determined considered the maximum bending deflection of samples (2μm). The dependences between stress and strain of microcantilever is presented in Fig.7 and of microbridge in Fig.8, respectively. The maximum bending stress of the microcantilever 250×30×1.9μm is estimated of 14.3MPa if the force is applied at the beam free-end. Of the investigated microbridge 250×30×1.9μm, a stress of 116.7MPa is determined if the force is applied at the beam mid-point and bends the sample to substrate.

Finite element analysis (FEA) is useful to estimate the stress distribution in microbridges and microcantilevers when the beams deflect completely to substrate. The forces used in the FEA are the mechanical forces coming from the experimental investigations given by the bending of AFM probe and its real stiffness. The modeling and FEA were performed using Oofelie::Multiphysics software driven by SAMCEF.

Figure 9 presents the finite element analysis and the distribution of the bending stress of investigated cantilevers. The thickness of microcantilevers is 1.9μm, the width of 30μm and the length of 250μm. The beam is deflected with 2 μm until substrate by a force applied at the beam free-end. The maximum bending stress of the cantilever corresponds to 15.36MPa.

The finite element analysis of the investigated microbridge is performed considering the experimental determined force, applied at the midpoint of samples. The samples are deflected with 2μm until substrate and the stress distribution is computed. The maximum bending stresses appear near anchor (in clamped region) and its value is 122.78MPa (Fig.10).

The FEA results of the bending stress are in good agreement with the experimental results. The differences between results are influenced by the following:

- the accuracy of experimental tests which depends on the testing conditions, on the initial calibration of AFM device and the type of AFM probe;
- the Young's modulus used in FEA is a theoretical one (which was taken from literature) and it differ from the experimental Young's modulus;
- the differences between theoretical dimensions of sample and the real dimensions (in the FEA the theoretical dimensions were used);
- the assumptions of the Euler-Bernoulli beam model used in (9) and (10) for analytical computation of stress [3, 9].

3. Dynamic investigations of electrostatically actuated MEMS components

The vibrating MEMS structures as microcantilevers and microbridges under electrostatic actuation are dynamic investigated in order to determine the frequency response of sample under a harmonic loading and the effect of the testing condition on velocity and amplitude of oscillations. In these studies, the lower electrode is positioned at the beam free-end for the investigated microcantilever and at the beam mid-point of microbridge as presented Fig.11.

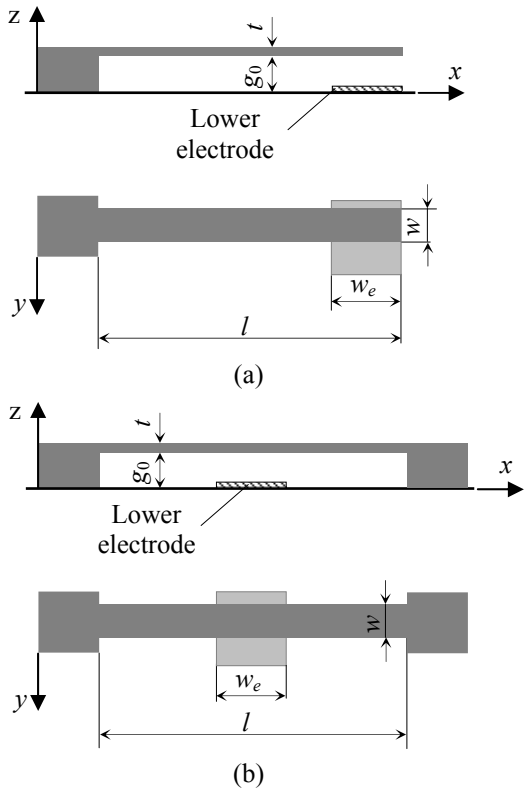

Fig.11. Schematic of a microcantilever (a) and a microbridge (b) under electrostatic actuation.

When a DC voltage (V_{DC}) is applied between lower electrode and the vibrating MEMS structure, an electrostatic force is set up and the cantilever bends downwards and come to rest in a new position. To drive the resonator at resonance, an AC harmonic load of amplitude V_{AC} vibrates the cantilever at the new deflected position.

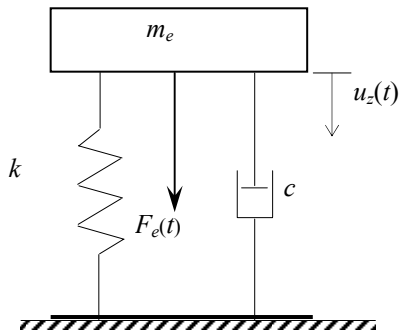

Fig.12. A single degree of freedom model used in the dynamic investigations of MEMS components.

A single degree of freedom model is used to simulate the dynamic response of the resonator due to the V_{DC} and V_{AC} electric loadings as presented in Fig.12. In this model the proof mass of the cantilever is modeled as a lumped mass m_e, and its stiffness is considered as a spring constant k. This part forms one side of a variable capacitor - the vibrating part. The bottom electrode is fixed and considered as the second part of the MEMS structure. If a voltage composed of DC and AC terms as:

$$V = V_{DC} + V_{AC}\cos(\omega t) \tag{16}$$

is applied between resonator electrodes, the electrostatic force applied on the structure has a DC component as well as a harmonic component with the frequency ω such as:

$$F_e(t) = \frac{\varepsilon A V^2}{2[g_0 - u_z(t)]^2} \tag{17}$$

where ε is the permittivity of the free space, $A=w_e*w$ is the effective area of the capacitor, g_0 is the initial gap between flexible plate and substrate, and $u_z(t)$ is the displacement of the mobile plate under the electrostatic force $F_e(t)$.

The expression (17) evidences two aspects: the electromechanical coupling between the instantaneous value of the beam gap (g_0 - u_z) and the applied voltage, then the nonlinear dependence on the mechanical displacement u_z and the voltage.

Pull-in voltage, at which the elastic stiffness does not balance the electric actuation and the beam tends to collapse, can be evaluated by funding the maximum gap allowing the static equilibrium. The spring force and the electrostatic actuation have opposite directions. Instability threshold is found by imposing the two conditions of null total force and the null derivative with respect to the displacement:

$$ku_z - \frac{\varepsilon A V^2}{2(g_0 - u_z)^2} = 0 \tag{18}$$

$$k - \frac{\varepsilon A V^2}{(g_0 - u_z)^3} = 0 \tag{19}$$

Unknown displacement and voltage are:

$$u_{pull-in} = \frac{g}{3} \tag{20}$$

$$V_{pull-in} = \sqrt{\frac{8}{27}\frac{g^3 k}{\varepsilon A}} \tag{21}$$

where $u_{pull-in}$ and $V_{pull-in}$ are the maximum displacement and voltage for which is possible to have a stable equilibrium configuration, k is the beam stiffness given by equation (1) for microcantilever and equation (2) for microbridge.

Dynamic analysis of electrostatically actuated microcomponents is performed by linearizing the electrostatic actuation around an equilibrium position. The equivalent stiffness of investigated MEMS resonator can be computed as:

- for microcantilever

$$k_{eff} = \frac{3EI_y}{l^3} - \frac{\varepsilon A V^2}{(g-u_z)^3} \tag{22}$$

- for microbridge

$$k_{eff} = \frac{192EI_y}{l^3} - \frac{\varepsilon A V^2}{(g-u_z)^3} \tag{23}$$

Based on these equations, the resonant frequency of electrostatically actuated microcantilever and microbridges can be computed as:

$$\omega_0 = \frac{1}{2\pi}\sqrt{\frac{k_{eff}}{m_e}} \tag{24}$$

where m_e is the equivalent mass of system.

Using the assumption that the kinetic energy of the distributed-parameter system is equal to the kinetic energy of the equivalent lumped – parameter mass, the equivalent mass can be determined [14]. The equivalent mass of a microcantilever is $0.235\times m$ and of a microbridge is $0.406\times m$ (m is the effective mass of beam).

The dynamic response of MEMS resonators presented in Fig.1 subjected to a harmonic electrostatic force F_e(t) with the driving frequency ω given by an AC voltage is governed by the equation of motion:

$$m\cdot\ddot{u}_z(t) + c\cdot\dot{u}_z(t) + k\cdot u_z(t) = F_e(t) \tag{25}$$

where c is the damping factor.

The response of system under DC and AC voltages is given by equation:

$$u_z(t) = \frac{u_z}{\sqrt{\left(1-\left(\frac{\omega}{\omega_0}\right)^2\right)^2 + \left(2\xi\frac{\omega}{\omega_0}\right)^2}} \tag{26}$$

where ξ is the damping ratio and ω_0 is the resonant frequency of beams given by equation (24).

Usually, the response is plotted as a normalized quantity $u_z(t)/u_z$. When the driving frequency equals the resonant frequency $\omega = \omega_0$, the amplitude ratio reaches a maximum value. At resonance, the amplitude ratio becomes:

$$\frac{u_z(t)}{u_z} = \frac{1}{2\xi} \tag{27}$$

An important qualifier of mechanical microresonators is the quality factor. At resonance, the quality factor Q is expressed as [14]:

$$Q_r = \frac{1}{2\xi} \tag{28}$$

and the normalized response given by equation (26) is exactly the equal to Q_r.

The quality factor is also called sharpness at resonance, which is defined as the ratio:

$$Q_r = \frac{\omega}{\omega_2 - \omega_1} \tag{29}$$

where (ω_2 - ω_1) is the frequency bandwidth which can be determined from the frequency response experimental curves.

The experimental investigations of the vibrating MEMS structures are performed using a vibrometer analyzer and a white noise signal. The aim of the experimental investigations is to determine the frequency response of the investigated microcantilever and microbridge and the effect of the operating conditions on the velocity and amplitude of oscillations.

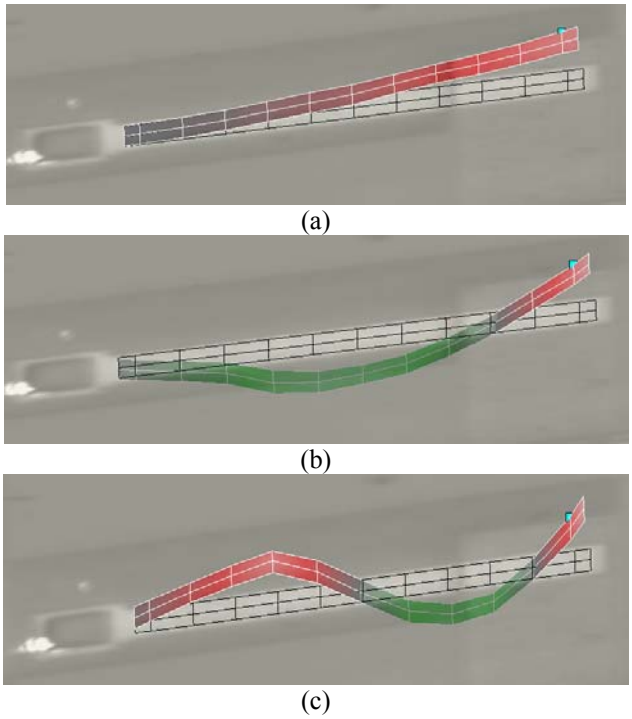

(a) (b) (c)

Fig.13 The first bending mode (a), the second bending mode (b) and the third bending (c) mode of oscillations of an electrostatically actuated MEMS cantilevers 250×30×1.9μm.

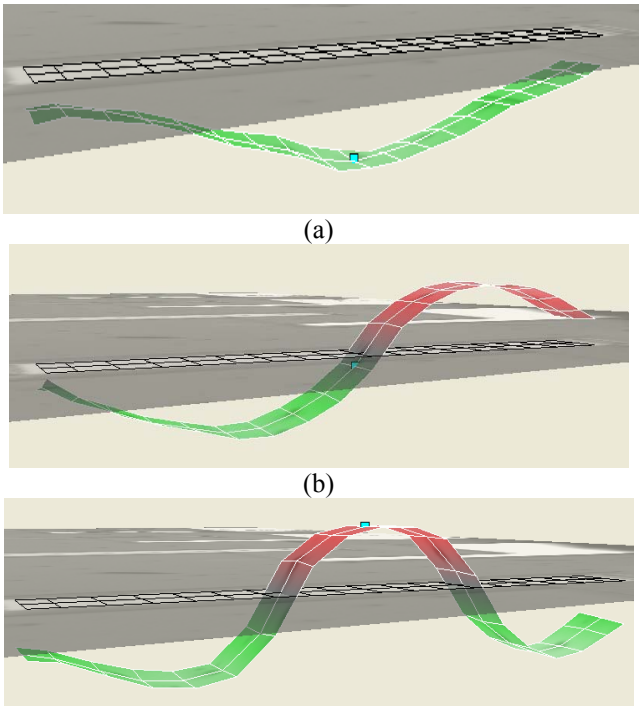

Fig.14 The first bending mode (a), the second bending mode (b) and the third bending mode (c) of oscillations of an electrostatically actuated MEMS microbridge 250×30×1.9μm

During experimental tests a DC offset signal of 5V and peak amplitude of 5V of the driving signal are applied to bend and oscillate the samples. The tests are performed under ambient conditions and in vacuum in order to estimate the effect of the damping on the velocity and amplitude of oscillations. Different vibration modes of samples can be visualized and analyzed. Figure 13 shows different bending modes for the microcantilever 250×30×1.9μm. The first bending mode of vibrations of the investigated microbridge 250×30×1.9μm is presented in Fig.14a, the second mode in Fig.14b, and the third mode in Fig.14c, respectively.

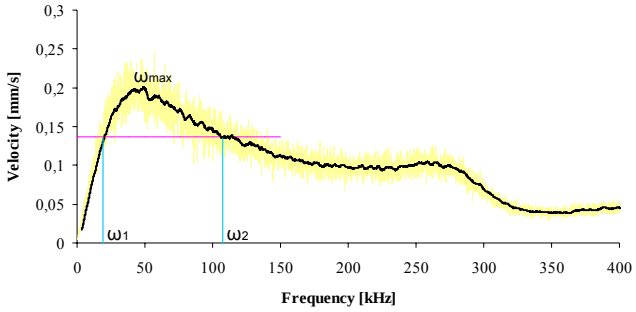

Fig.15. The first frequency response of an electrostatically actuated MEMS microcantilever 250×30×1.9μm tested in ambient conditions.

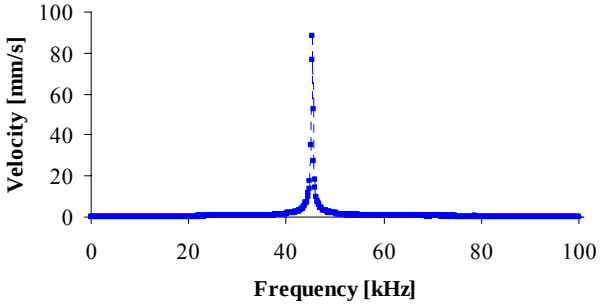

Fig.16. The first frequency response of an electrostatically actuated MEMS microcantilever 250×30×1.9μm tested in vacuum (4×10^{-4}mbar).

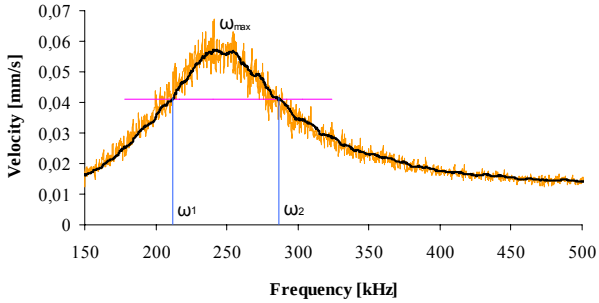

Fig.17. The first frequency response of an electrostatically actuated MEMS microbridge 250×30×1.9μm tested in ambient conditions.

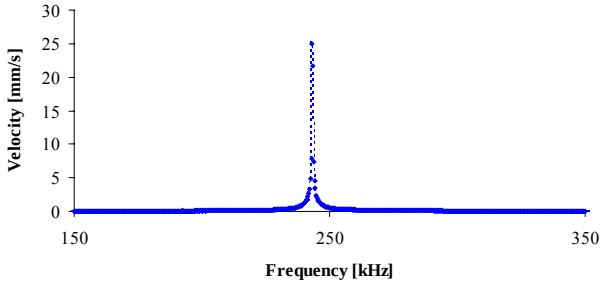

Fig.18. The first frequency response of oscillations of an electrostatically actuated MEMS microbridge 250×30×1.9μm tested in vacuum (4×10^{-4}mbar).

In order, to analyze the dynamic response of investigated MEMS components only the first bending mode of oscillations is monitored and analyzed. The frequency response curves of the investigated microcantilever and microbridge tested in air are presented in Figs.15 and 17. Figures 16 and 18 present the frequency response of the same beams tested under vacuum conditions. The experiments were repeated 10 times for each of samples and the average results are considered. The dynamic experimental characteristics of the investigated microbridge and microcantilever are presented in the next table.

Table 1 The dynamic characteristics of investigated MEMS components as a function of the testing conditions.

Samples 250×30×1.9μm	RF [kHz]	Velocity [mm/s]		Amplitude [nm]	
		air	vacuum	air	vacuum
Cantilever	45.3	0.19	90	0.066	316
Microbridge	243	0.058	25	0.046	18

Additionally, the resonant Q-factor of the investigated samples can be estimated based on the frequency response curve obtained under ambient conditions. The frequency bandwidth ω_2-ω_1 is determined from the frequency response curves (Figs.15 and 17). The quality factor at resonance is then computed based on equation (29). A quality factor of 0.51 is obtained for the microcantilever tested in ambient conditions and 3.24 for the investigated microbridge. Using the relation (28), the damping ratio of samples tested in ambient conditions can be estimated. A damping ration of 0.98 is determined for the microcantilever and 0.15 of the investigated microbridge. The damping ratio ξ is any positive real number. For value of the damping ratio $0 \leq \xi < 1$ as in the experiments, the system has an oscillatory response.

The difference between the shape of the frequency response curves of samples tested in ambient conditions and the same samples tested in vacuum is given by the damping effect. In vacuum the damping effect given by air is low and the quality factor has a high value. This has influence of the velocity and amplitude of oscillations which increasing under the same input voltage if the samples are tested in vacuum.

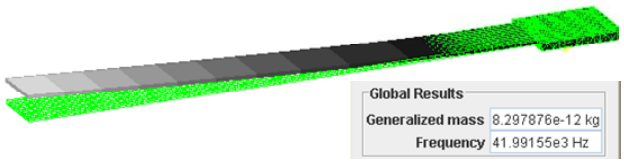

Fig.19. Modal finite element analysis of a microcantilever 200×30×1.9μm.

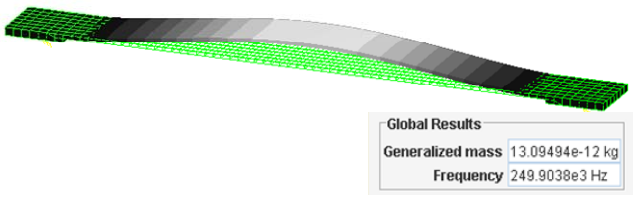

Fig.20. Modal finite element analysis of a microbridge 200×30×1.9μm.

Using the Oofelie:Multiphysics software, the coupling field between the electrostatic actuation and the mechanical response of structure is simulated. The FEA results give information about the resonant frequency response of beam. The resonant frequency is determined at 41.99kHz for the investigated microcantilever (Fig.19) and of 249.9kHz for microbridge (Fig.20).

4. Stiction and friction of MEMS materials

Stiction is the adhesion of contacting surfaces due to surface forces, which mainly contain capillary forces, van der Waals forces, Casimir forces and electrostatic forces. Adhesion forces between different MEMS materials can be measured using the spectroscopy mode of AFM [2, 5, 15-17]. The adhesion between the AFM tip material and MEMS materials can overwhelm the other forces at play. The lateral mode of atomic force microscope is a well method to estimate the nanofriction [2, 5].

In this paper, the adhesive effects between AFM tip (Si_3N_4) and MEMS materials are evaluated using the spectroscopy mode of AFM. The force spectroscopy AFM curves give the direct measurement of tip-sample interaction forces as a function of the gap between the tip and sample. The adhesion between tip and sample is characterized by so-called pull-off or pull-out force. The pull-off force is related in current continuum contact mechanics model to the work of adhesion.

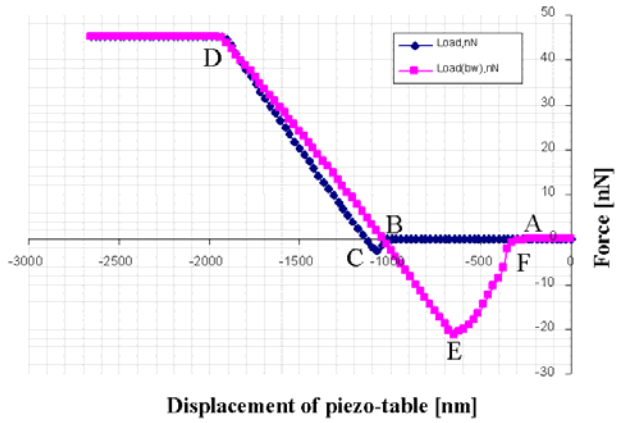

Fig.21. Force versus AFM piezo-table displacement during experimental test of the contact between AFM tip Si_3N_4 and a gold material.

During experimental tests the sample is moved up and down (in and out of contact with the tip) and a dependence curve between displacements of piezo-table versus deflection of AFM probe is obtained. Using the known stiffness of AFM probe, the dependence between displacements of piezo-table and force is plotted as presented in Fig.21. During the approach (A–B) no interactions occur between the tip and the sample surface. As the tip-surface distance becomes sufficiently small, the gradient of the attractive force overcomes the cantilever spring constant and brings the tip in contact with the sample surface (position C). Further approaching causes a deflection of the cantilever (position C–D). The unloading part of the force–displacement curve starts from position D, the deflection of the cantilever is decreased as the sample surface retracts from the tip. When the sample

surface is further withdrawn from the tip, the cantilever is deflected owing to adhesive forces. At position E, the elastic force in the cantilever overcomes the force gradient and the tip snaps off from the surface (position F). From position F to A, the cantilever returns to its equilibrium position.

The AFM probe has the stiffness 0.3N/m and using the experimental AFM values the dependence between force of AFM probe and displacement of piezo-table was computed for three materials used in MEMS as polysilicon, gold and aluminum. The maximum adhesion force between the AFM tip (Si_3N_4) and the samples are 26nN for polysilicon, 21nN for gold and 37nN for aluminum.

The friction coefficient is estimated by AFM measurements of frictional force. In that case, the two surfaces in contact are the tip of AFM probe and the sample. This measurement provides an index of friction behavior between two materials being in contact and in relative motion. The relative motion between tip and surface is realized by a scanner composed of piezoelectric elements, which move the material surface perpendicular to the tip of the AFM probe with a certain periodicity. The scanner can also be extended or retracted in order to modify the normal force applied to the surface. If the normal force increases while scanning because the surface is not flat, the scanner is retracted by a feedback loop. On the other hand, if the normal force decreases, the surface is brought closer to the tip by extending the scanner. The relative sliding of the AFM probe tip on the top surface of samples is influenced by friction. The lateral force, which acts in the opposite direction of the scan velocity, causes torsion of the AFM probe. Normal and friction forces being applied at the tip-sample interface are measured using the laser beam deflection technique.

The following relationship exists at micro/nano scale between the friction force F_f and the normal load [2, 15]:

$$F_f = \mu(F_N + F_a) \tag{30}$$

where μ is the friction coefficient, F_N is the force given by the bending of AFM probe and F_a is the adhesion force between the sample surface and the AFM tip.

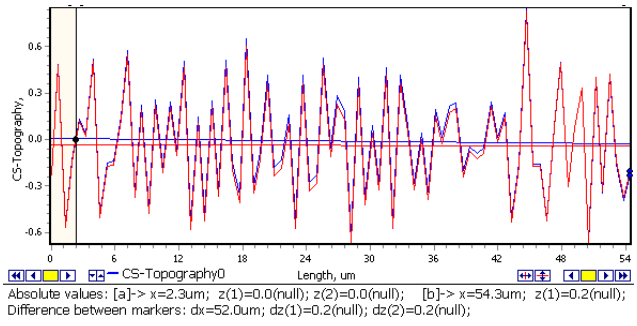

Fig.22. Deflection of AFM probe during lateral movement on a polysilicon surface.

The AFM probe is moving in lateral direction on sample and rotational deflections *dz* of AFM probe is obtained from the friction map as presented in Fig.22. These rotational deflections of the AFM probe are proportional with the friction forces between the AFM probe (Si_3N_4) and samples.

Based on the rotational deflection *dz* of the AFM probe the friction force is computed as:

$$F_f = \frac{dz \cdot r \cdot G \cdot h^3 \cdot b}{l^2 \cdot s} \tag{31}$$

where *dz* is the calibrated deflection of AFM cantilever [nm], *r* =0.33, *G* – shear modulus of the cantilever material, *l* – length of AFM probe, *h* – thickness of AFM probe, *b* – width of AFM probe, *s* - height of tip of AFM probe.

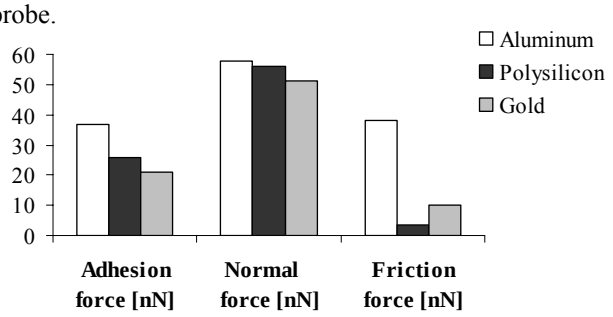

Fig.23. Experimental forces of the contact between the AFM tip (Si_3N_4) and the investigated MEMS materials.

Using relation (31), the friction forces between the AFM probe and the investigated MEMS materials are determined. The normal force is computed based on the bending deflection of AFM probe and its real stiffness. These values are presented in Fig.23 as well as the adhesion forces. Using equation (30) the friction coefficient is estimated of 0.04 between Si_3N_4 and polysilicon, of 0.14 between Si_3N_4 in contact with gold and of 0.4 between Si_3N_4 and aluminum.

5. Conclusion

In this paper, theoretical formulas, experimental models and finite element analysis are presented in order to determine the mechanical and tribological characteristics of MEMS components.

Mechanical studies are developed by considering microcantilevers and microbridges fabricated from polysilicon as flexible MEMS components. The other materials for interests, used in tribological investigations are gold and aluminum. In biological and chemical MEMS applications, the gold and aluminum microstructures are crucial for surface stress – based biochemical detections. Moreover, the gold coating is ideal for strong anchorage of proteins and nucleic acids by self-assembly chemistry.

The atomic force microscope is a well technique used to estimate the mechanical properties at nano-scale. The accuracy of the experimental investigations strongly depends by the initial calibration of AFM probe. The theoretical and experimental results of stiffness, modulus

of elasticity, stress and strain are in good agreement with theoretical and finite element analysis results.

Dynamical analyses presented in this paper were developed using electrostatically actuated MEMS resonator. Frequency response, velocity and amplitude of oscillations were experimentally determined under ambient conditions and in vacuum. The damping effect given by air has a big influence on amplitude and velocity of oscillations. The quality factor of a microbridge tested in air is about 6 times larger than the quality factor of a microcantilever fabricated in the same geometrical dimensions. The sensitivity, amplitude and velocity of oscillations of a microcantilever are higher than to a microbridge for the same operating conditions.

The frequency responses of investigated beams, experimentally obtained using a Polytec Vibrometer, are close to the results of finite element simulations.

Generally, coefficients of friction on the nanoscale differ by the macroscale. The adhesion force has a big influence on stiction and friction.

Mechanical properties of MEMS structures address a few issues as: the reliability of structure used under various loading conditions and in different environments; the performance of movable MEMS components under tribological conditions as wear, friction, stiction, environmental effects; the reliability of microcomponents under cyclical loading with a big influence on the MEMS lifetime.

Acknowledgments

The authors would like to acknowledge the financial support of the Ministère de la Région Wallonne, Division de la Recherche et de la Coopération Scientifique in the framework of the research program FIRST Post-Doc n° 616365 (MOMIVAL). The financial support of the Romanian National Authority for Scientific Research, CNCS-UEFISCDI, project number PN-II-RU-TE-2011-3-0106 is also gratefully acknowledged.

References

[1] S.M. Allameh, J. Matter. Sci. **38**, 4115 (2003).
[2] B. Bhushan (Ed), Handbook of Nanotribology and Nanomechanics – An Introduction, Berlin (2005).
[3] N. Lobontiu, E. Garcia, Mechanics of MEMS, New York (2004).
[4] W. Merlijn van Spengen, J. Microelec. Reliab. **43**, 1049 (2003).
[5] M. Pustan, Z. Rymuza, Mechanical and Tribological Characterizations of MEMS Structures, Cluj Napoca (2007).
[6] G. De Pasquale, A. Soma, A. Ballestra, J. Analog Integr. Circ. Sig. Process **61**, (2009).
[7] A.Y. Suh, A.A. Polycarpou, J. of Trib. **125** (2003).
[8] Y. Li, Z. Jiang, An overview of reliability and failures mode analysis of MEMS. In Handbook of Performability Engineering, London (2008).
[9] M. Pustan, Z. Rymuza, J. Micromech. Microeng. **17**, 1611 (2007).
[10] M. Pustan, G. Ekwinski, Z. Rymuza, Int. J. Mater. Res **5**, 384 (2007).
[11] H. Kahn, R. Ballarini, A.H. Heuer, Solid State and Mat. Sci. **8** (2004).
[12] A. B. O. Soboyejo, K. D. Bhalerao, W. O. Soboyejo, J. Mat. Science **38,** 4163 (2003).
[13] M. Pustan, Dig. J. Nanomat. Biostr. **6**(1), 285 (2011).
[14] N. Lobontiu, Dynamics of Microelectromechanical Systems, New York, 2007.
[15] M. Pustan, O. Belcin, J. Tribology in Industry **31,** 43 (2009).
[16] B. Bhhusan, Wear **251**, 1105 (2001).
[17] A.Y. Suh, A.A. Polycarpou, J. of Trib. **125** (2003).

*Corresponding author: Marius.Pustan@omt.utcluj.ro